

# Structural and soft magnetic properties of a new nanocrystalline Fe-based and B-free alloy

Jianguo Long,<sup>a)</sup> D. E. Laughlin, and M. E. McHenry

Department of Material Science and Engineering, Carnegie Mellon University, Pittsburgh, Pennsylvania, 15213 USA

(Presented on 9 November 2007; received 10 September 2007; accepted 3 October 2007; published online 23 January 2008)

A new nanocrystalline Fe-based soft magnetic alloy is discussed here. Ingots of nanocrystalline alloys  $(\text{FeCu})_{80}\text{Zr}_x\text{Si}_{20-x}$  ( $x=5, 6, \text{ and } 8$ ) were prepared by arc melting. The ingots were remelted and cast into  $25\text{--}30\ \mu\text{m}$  thick ribbons by a single roller melt spinning method. X-ray diffraction (XRD) revealed the as-spun ribbons to be amorphous. The structural evolution of these samples was studied by XRD and transmission electron microscopy (TEM) after annealing at 450, 480, and 550 °C. XRD shows the primary nanocrystallization product to be the  $\alpha\text{-Fe}(\text{Si})$  phase. The grain size was observed by TEM to be  $\sim 10\ \text{nm}$  after annealing at 480 °C for 1 h and 14 nm after 550 °C for 1 h. ac soft magnetic properties were measured using a Walker AMH 401 ac permeameter. The core loss at an exciting frequency  $f=100\ \text{kHz}$  and maximum induction  $B_m=1\ \text{kG}$  was determined to be less than 19 W/kg. © 2008 American Institute of Physics. [DOI: 10.1063/1.2829396]

## INTRODUCTION

Nanocomposite soft magnetic materials have been studied over the past several decades due to their excellent soft magnetic properties. These allow for their use in technical applications such as magnetic sensors and cores. After partially crystallization at their primary crystallization temperature, the alloys develop a nanosized ferromagnetic phase  $\text{DO}_3\text{-FeSi}$  (Finemet),<sup>1</sup>  $\alpha\text{-Fe}$  (Nanoperm),<sup>2</sup> or  $\alpha\text{-FeCo}$  (Hitperm) (Ref. 3) surrounded by an amorphous matrix. The excellent soft magnetic properties are ascribed to ferromagnetic nanocrystals being smaller than exchange correlation length.<sup>4,5</sup> Until now, all known technically important nanocomposite soft magnetic alloys and their derivatives include boron.<sup>6</sup> Boron is necessary as a glass former to prevent crystallization and forming undesirably large grains. Boron increases the glass forming ability and improves its thermal stability. Despite these benefits, boron is a relatively expensive element. Therefore, boron-free alloys with properties comparable to those that contain boron would be of great economical advantage.

To obtain the low boron or boron-free amorphous alloys with equivalent soft magnetic properties as other commercial soft magnetic alloys, multicomponent alloys which combine the desirable features of Fe-TM (TM=early transition metal) and Fe-Si alloys are chosen as a starting point. Early transition metals serve as an effective element for impeding grain growth in nanocomposite soft magnetic materials. The Fe-TM binary system also has a strong glass forming ability since alloys such as Fe-Zr, Fe-Hf, etc., have relatively deep eutectics. The eutectic point is near the composition  $\text{Fe}_{90}\text{Zr}_{10}$ , in Fe rich region of the Fe-Zr binary phase diagram. It is therefore possible to maintain the high magnetic moment in the amorphous alloy because of the high Fe content. Early research on this alloy system showed an amorphous phase to

be produced for alloys as high in Fe content as  $\text{Fe}_{93}\text{Zr}_7$ .<sup>7-11</sup> Ramanan and Fish<sup>12</sup> observed that replacement of B by Si increases activation energy barriers in Metglas alloys. The influences of alloy composition on nanocrystallization kinetics are reviewed by McHenry *et al.*<sup>13</sup>

In this paper, we produced precursor amorphous alloys in Fe-Zr-Si system by rapid solidification. Subsequently, we obtained the nanocomposite soft magnetic alloy from these amorphous alloys by primary crystallization. The detailed structure and magnetic properties will be discussed below.

## EXPERIMENTAL

Fe (99% pure), Zr (99% pure), FeSi (99% pure) and Cu (99.9% pure) were mixed and melted in arc melter to produce  $\text{Fe}_{80}(\text{Zr}_x\text{Si}_{20-x})\text{Cu}_1$  alloy ingots with  $x=5\text{--}10$ . Amor-

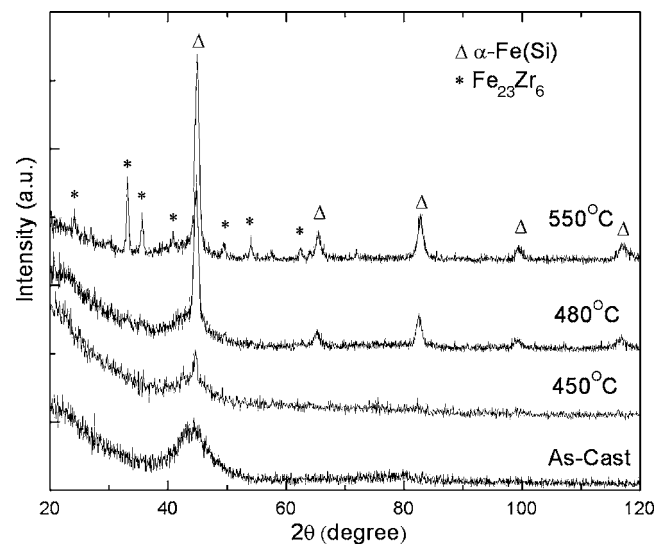


FIG. 1. XRD patterns of an amorphous  $\text{Fe}_{79}\text{Zr}_5\text{Si}_{15}\text{Cu}_1$  alloy and after annealing at 450, 480, and 550 °C for 1 h.

<sup>a)</sup>Electronic mail: jianguo@andrew.cmu.edu.

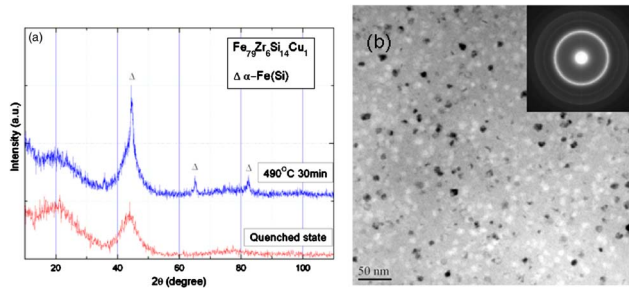


FIG. 2. (Color online) XRD pattern and TEM bright field image of the  $\text{Fe}_{79}\text{Zr}_6\text{Si}_{14}\text{Cu}_1$  alloy annealed at  $490^\circ\text{C}$  for 30 min.

phous ribbons, 25–30  $\mu\text{m}$  thick and  $\sim 3$  mm wide, of nominal composition  $\text{Fe}_{80}(\text{Zr}_x\text{Si}_{20-x})\text{Cu}_1$  were prepared by the single roller melt spinning. Alloy ingots of various compositions were induction melted in a quartz crucible and cast in argon onto a copper wheel rotating at  $\sim 50$  m/s. The amorphous samples were subsequently crystallized by sealing them in evacuated silica tubes, placing them in a preheated furnace at prescribed temperatures for one hour, and then water quenched to room temperature.

A detailed structure analysis as a function of annealing temperature was performed by x-ray diffraction (XRD) with  $\text{Cu } K\alpha$  radiation. A JEOL JEM2000 transmission electron microscope operated at 200 keV was employed to characterize the microstructure. Transmission electron microscopy (TEM) samples were prepared by mechanical polishing and ion milling. Magnetization was measured using a Lakeshore vibrating sample magnetometer and ac magnetic property measurements were performed at room temperature using a Walker Scientific AMH 401 ac permeameter.

## RESULTS AND DISCUSSION

Figure 1 shows the x-ray diffraction patterns, measured at room temperature, of a  $\text{Fe}_{79}\text{Zr}_5\text{Si}_{15}\text{Cu}_1$  alloy in its as-quenched state and the nanocomposite state after annealing at 450, 480, and  $550^\circ\text{C}$  for 60 min. Only one broad peak in the XRD pattern is observed in the as-quenched state indicating that to the resolution of XRD, the quenched state is amorphous. The broad peak sharpens after annealing at  $450^\circ\text{C}$  for 1 h due to nanocrystallization. XRD results show the primary crystallization product to be nanocrystalline

$\alpha\text{-Fe}(\text{Si})$ . The sample annealed at  $480^\circ\text{C}$  for 1 h consisted of the  $\alpha\text{-Fe}(\text{Si})$  and the amorphous matrix. According to the Scherrer equation,<sup>14</sup>

$$D = \frac{0.9\lambda}{B \cos(\theta)},$$

where  $\lambda$  is the wave length of incident x rays,  $B$  is the full width at half maximum of the diffraction peak, and the average grain size of sample annealed at  $480^\circ\text{C}$  for 60 min is determined to be  $\sim 10$  nm. In the sample annealed at  $480^\circ\text{C}$ , only the primary crystalline  $\alpha\text{-Fe}(\text{Si})$  phase was observed, however, with annealing temperature higher than the secondary crystallization temperature; the secondary  $\text{Fe}_{23}\text{Zr}_6$  phase was also observed (see the diffraction pattern of sample annealed at  $550^\circ\text{C}$ ), as shown in Fig. 1.

Figure 2 shows the x-ray diffraction pattern and a TEM bright field image of a  $\text{Fe}_{79}\text{Zr}_6\text{Si}_{14}\text{Cu}_1$  alloy after annealed at  $490^\circ\text{C}$  for 30 min. The broad amorphous peak in the XRD data becomes sharp after annealed at  $490^\circ\text{C}$  for 30 min with the appearance of the primary crystallization product. The sample annealed at  $490^\circ\text{C}$  for 30 min consisted of the  $\alpha\text{-Fe}(\text{Si})$  primary crystallization phase and the amorphous matrix. The bright field image of the sample annealed at  $490^\circ\text{C}$  for 30 min in Fig. 2(b) shows the average primary nanocrystal size to be  $\sim 7$  nm. The diffuse halo ring of the electron diffraction pattern is due to the residual amorphous matrix in the nanocomposite sample.

To observe nanocrystallite grain's size as a function of annealing temperature, we annealed samples at 450, 480, and  $550^\circ\text{C}$  for 1 h, respectively. Figure 3 shows bright field images of these samples. The average nanocrystallite size determined by dark field images was 8 nm for  $450^\circ\text{C}$ , 10 nm for  $480^\circ\text{C}$ , and 14 nm for  $550^\circ\text{C}$ . Although the nanocrystallite size increases slightly with the annealing temperature, the number density of the nanocrystals increases more significantly.

In Finemet nanocomposite soft magnetic alloys, Cu has been determined to act as a nucleation agent<sup>15,16</sup> for  $\text{DO}_3\text{-Fe}_3\text{Si}$  nanocrystals during the primary crystallization process. We have introduced Cu into our alloy to also serve as a nucleation agent. The proof of its efficacy is shown in Fig. 4. A Cu-free alloy with chemical composition  $\text{Fe}_{80}\text{Zr}_6\text{Si}_{14}$  was melt spun for comparison with the effect of Cu additions to a similar alloy. Figure 4 shows the bright

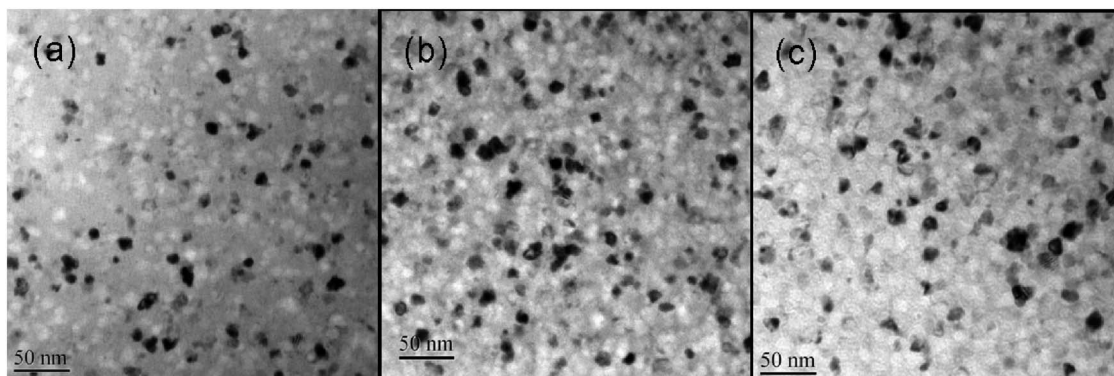


FIG. 3. Bright field image of the  $\text{Fe}_{79}\text{Zr}_5\text{Si}_{15}\text{Cu}_1$  alloy annealed at (a)  $450^\circ\text{C}$ , (b)  $480^\circ\text{C}$ , and (c)  $550^\circ\text{C}$  for 1 h.

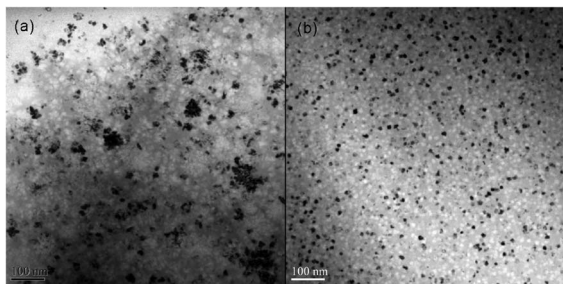


FIG. 4. Bright Field image of the (a)  $\text{Fe}_{80}\text{Zr}_6\text{Si}_{14}$  and (b)  $\text{Fe}_{79}\text{Zr}_6\text{Si}_{14}\text{Cu}_1$  alloys. Both are annealed at  $500^\circ\text{C}$  for 30 min.

field image of the samples annealed at  $500^\circ\text{C}$  for 30 min. The alloy with Cu additions ( $\text{Fe}_{79}\text{Zr}_6\text{Si}_{14}\text{Cu}_1$ ) has fine grains and a uniform grain size distribution ( $8.1 \pm 0.9$  nm) (Fig. 4). So Cu is seen to be effective in controlling the grain size and shape in these alloys.

To measure the ac soft magnetic properties, a  $25\ \mu\text{m}$  thick amorphous ribbon having a composition of  $\text{Fe}_{79}\text{Zr}_5\text{Si}_{15}\text{Cu}_1$  was wound to form the toroidal cores of external diameter of 22 mm, internal diameter of 18 mm, and height of 3 mm. The toroidal cores were annealed at various annealing temperatures. Figure 5 shows a  $BH$  loop under the measurement condition of  $H_{\text{max}} = 10$  Oe and  $f = 1$  kHz for the sample annealed for 2 h at  $460^\circ\text{C}$ . The detailed core loss data are shown in Fig. 6. The coercivity at  $f = 1$  kHz is 5 A/m and  $P_{0.1/100}$ , where  $P_{0.1/100}$  represents the core loss under the condition of  $B_{\text{max}} = 1$  kG and  $f = 100$  kHz, is about 18.5 W/kg, which is close to the core loss of Finemet ( $P_{0.1/100} = 12$  W/kg for Finemet).

## CONCLUSION

A new nanocomposite soft magnetic material was developed in the Fe–Zr–Si–Cu alloy system. Structural analysis shows the primary crystallization products to consist of ultrafine nanocrystals embedded in a residual amorphous matrix. These ultrafine nanocrystals have round shapes and a

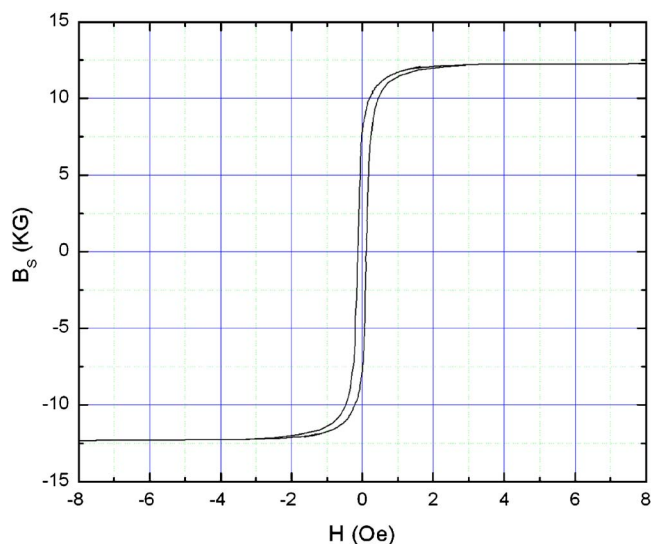


FIG. 5. (Color online)  $B$ - $H$  loop measured at  $f = 1$  kHz for the  $\text{Fe}_{79}\text{Zr}_5\text{Si}_{15}\text{Cu}_1$  alloy annealed at  $460^\circ\text{C}$  for 2 h.

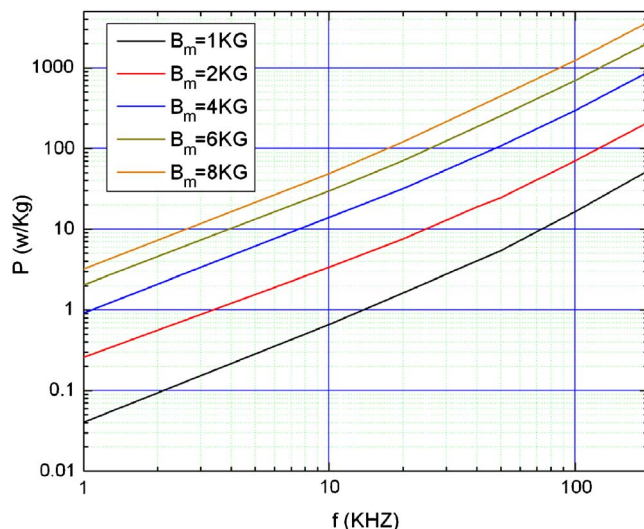


FIG. 6. (Color online) Core loss vs frequency plot of the  $\text{Fe}_{79}\text{Zr}_5\text{Si}_{15}\text{Cu}_1$  alloy annealed at  $460^\circ\text{C}$  for 2 h.

uniform grain size distribution ( $8.1 \pm 0.9$  nm after annealing at  $490^\circ\text{C}$  for  $\text{Fe}_{79}\text{Zr}_6\text{Si}_{14}\text{Cu}_1$ ), which are key factors to achieving low coercivity. Moreover, these alloys have relatively low core loss as compared with the commercial nanocomposite soft magnetic materials. We conclude that the Fe–Zr–Si–Cu alloy studied here is a good candidate for economical soft magnetic material applications.

## ACKNOWLEDGMENTS

This work was supported by National Science Foundation under Grant No. DMR-0406220. This work was also supported in part by the Army Research Laboratory and was accomplished under Cooperative Agreement No. W911NF-04-2-0017.

- <sup>1</sup>Y. Yoshizawa, S. Oguma, and K. Yamauchi, *J. Appl. Phys.* **64**, 6044 (1988).
- <sup>2</sup>K. Suzuki, N. Ktaoka, A. Inoue, A. Makino, and T. Masumoto, *Mater. Trans., JIM* **31**, 743 (1990).
- <sup>3</sup>M. A. Willard, D. E. Laughlin, M. E. McHenry, D. Thoma, K. Sickafus, J. O. Cross, and V. G. Harris, *J. Appl. Phys.* **84**, 6773 (1998).
- <sup>4</sup>G. Herzer, *IEEE Trans. Magn.* **25**, 3327 (1989).
- <sup>5</sup>G. Herzer, *IEEE Trans. Magn.* **26**, 1397 (1990).
- <sup>6</sup>M. E. McHenry, M. A. Willard, and D. E. Laughlin, *Prog. Mater. Sci.* **44**, 291 (1999).
- <sup>7</sup>C. L. Chien and K. M. Unruh, *Nucl. Instrum. Methods Phys. Res.* **199**, 193 (1982).
- <sup>8</sup>D. H. Ryan and J. M. Coey, *Phys. Rev. B* **35**, 8630 (1987).
- <sup>9</sup>T. Masumoto, K. Esashi, and M. Nose, U.S. Patent No. 4,623,387 (Nov. 18, 1986).
- <sup>10</sup>T. Masumoto, K. Esashi, and M. Nose, U.S. Patent No. 4,842,657 (Jun. 27, 1989).
- <sup>11</sup>K. M. Unruh and C. L. Chien, *J. Magn. Magn. Mater.* **31–34**, 1587 (1983).
- <sup>12</sup>V. R. V. Ramanan and G. Fish, *J. Appl. Phys.* **53**, 2273 (1982).
- <sup>13</sup>M. E. McHenry, F. Johnson, H. Okumura, T. Ohkubo, V. R. V. Ramanan, and D. E. Laughlin, *Scr. Mater.* **48**, 881 (2003).
- <sup>14</sup>M. DeGraef and M. E. McHenry, *Structure of Materials: An Introduction to Crystallography, Diffraction and Symmetry* (Cambridge University Press, Cambridge, 2007), p. 318.
- <sup>15</sup>J. D. Ayers, V. G. Harris, J. A. Sprague, W. T. Elam, and H. N. Jones, *Acta Mater.* **46**, 1861 (1998).
- <sup>16</sup>K. Hono, K. Hiraga, Q. Wang, A. Inoue, and T. Sakurai, *Acta Metall. Mater.* **40**, 2137 (1992).